PAPER

NJC
www.rsc.org/njc

# Indium nitride from indium iodide at low temperatures: synthesis and their optical properties

**Changzheng Wu,[b] Tanwei Li,[b] Lanyu Lei,[b] Shuangquan Hu,[b] Yi Liu[b] and Yi Xie*[ab]**

[a] *School of Chemical and Material Engineering, Southern Yangtze University, Wuxi, Jiangsu 214036, P.R. China*

[b] *Nano-materials and Nano-chemistry, Hefei National Laboratory for Physical Sciences at Microscale, University of Science & Technology of China, Hefei, Anhui 230026, P. R. China. E-mail: yxielab@ustc.edu.cn; Fax: +86-551-3603987; Tel: +86-551-3603987*

***Received (in Montpellier, France) 21st July 2005, Accepted 24th August 2005***
***First published as an Advance Article on the web 26th September 2005***



In this paper, we present an effective synthetic protocol to produce high quality InN nanocrystals using indium iodide ($InI_3$), one member of the family of indium halides, as the indium source at a low temperature of $<250$ °C (far below the decomposition temperature of InN). Notably, reports on InN synthesized from indium halides are rare due to the lack of well-defined synthetic protocols. Here, indium iodide ($InI_3$), with a stronger covalent ability, can also prevent the $In^{3+}$ from being reduced to elemental indium, and then InN is formed. This synthetic protocol not only provides an alternative method to successfully synthesize high-quality InN, but is also useful to fabricate other functional materials by using stronger covalent reactants to prevent reduction/oxidation in the oxidation/reduction reaction process, respectively. Furthermore, we also report the first example of an orientation–attachment process occurring between the metal nitride particles. The high purity of the InN nanoparticles can be seen from the XPS and HRTEM results, showing the as-obtained products possess no obvious iodine or amorphous layers on the surface of particles, respectively. By controlling the parameters of reaction temperature and time, nanoparticles with different sizes were obtained as the final products. Raman and IR results indicate that our experimental data were consistent with the theoretical prediction and this gives further evidence that high quality InN nanocrystals were obtained. Moreover, it has been shown that the near-infrared band around 0.7 eV is characteristic of these samples and there were no obvious peaks around 1.9 eV, indicating that these InN nanocrystals exhibit a band gap of 0.7 eV, rather than the previously accepted 1.9 eV.

## Introduction

The group III nitrides GaN, InN, $In_nGa_{1-n}N$, and $Al_nGa_{1-n}N$ have recently acquired technological importance for blue/violet LED and laser diode applications.[1] InN is especially interesting because its bandgap has recently been remeasured as 0.7 eV rather than the previously accepted 1.9 eV[2] and theoretical support for the new value has been provided.[3] Thus, nanoparticles of InN would be expected to have bandgaps varying from the near-infrared region of the electromagnetic spectrum, close to wavelengths of especial interest in telecommunications, through much of the visible region. Although InN possesses very attractive properties, it has not received as much attention as GaN and AlN. This is probably due to difficulties in growing high quality crystalline InN samples. InN is no different from GaN and AlN in the sense that it suffers from the same lack of a suitable substrate for epitaxial growth and, in particular, a high native defect concentration. In addition, due to its poor thermal stability, decomposing with loss of $N_2$ at low temperatures (427–550 °C),[4] InN cannot be grown at temperatures higher than 600 °C without extraordinarily high overpressure, which makes the growth of crystalline InN-containing materials challenging.[5]

Efforts for the low-temperature synthesis of crystalline InN below 300 °C, which is well below its decomposition temperature, can be simply classified into two sorts. One is to apply complexes or organometallic precursor compounds as precursors to produce InN nanocrystals in the liquid phase. For example, in the decomposition of azido precursor $Pr^i_2InN_3$, a solution–liquid–solid (SLS) process gave rise to InN fibers with diameters of *ca.* 20 nm diameter.[6] Decomposition of another azido precursor $[InN_3(CH_2\ CH_2\ CH_2NMe_2)_2]$ in trioctylphosphine oxide yielded cubic InN nanoparticles.[7] These precursor routes are very useful but there are some limitations to their realization because they require extreme reaction conditions such as an absolute nonaqueous, non-oxygen environment and the risk of azide explosion. The other method is the direct reaction of inorganic indium compounds and a nitrogen source. In this case, with the strong covalent ability of $In_2S_3$ to prevent the reduction of $In^{3+}$ to elemental indium, the reaction of $In_2S_3$ and $NaNH_2$ successfully yielded hexagonal nanocrystals with the diameters of 10–30 nm.[8] However, unlike the conventional routes for preparing other nitrides from its metal halides counterparts,[9] crystalline high-quality InN seems to be difficult to obtain from the direct reaction of corresponding indium halides precursors with nitrogen sources. As is reported, InN could not be obtained by the reaction of $Li_3N$ and $InX_3$ (X = Cl, Br), which yielded InX and elemental indium.[10] A later report stated that nanocrystals of InN with a mixture of cubic and hexagonal phases can be obtained from $InCl_3$ and $Li_3N$, but the evidence of the XRD pattern clearly indicated that the product is in fact a mixture of In and $In_2O_3$.[11] Using $InI_3$ as the In source, the given ratio of the mixed nitrogen source of $Li_3N$, $LiNH_2$, $NH_4Cl$ leads to InN and metallic In by the metathesis reactions,[12] however, the In metal seems to be inevitable in the final products and thus decreases the yield of InN. Here, a question emerged: is it possible for high-quality InN to be synthesized from indium

DOI: 10.1039/b510426b

halides? The positive answer will be found in the present work using $InI_3$. Concerning the four kinds of indium halides, $InF_3$, $InCl_3$, $InBr_3$, and $InI_3$, $InI_3$ has a stronger covalent ability than the other three. As is known, when two atoms form a chemical bond, the greater the difference between the electronegativity values for the two atoms, the more ionic the chemical bond between them.[13] The difference in electronegativity value between In and I is 0.88 (based on Pauling data), which is smaller than that for In and Br (1.18), In and Cl (1.38), In and F (2.20), verifying the stronger covalent ability of $InI_3$. Thus, $InI_3$, as one member of the family of indium halides, is more likely to be useful for obtaining high-quality InN, since the stronger covalency of $InI_3$ can also prevent the $In^{3+}$ being reduced to elemental indium. If this is so, then it will facilitate the synthesis of high-quality InN, which is of scientific and technical interest from a synthetic-chemistry point of view. Herein, reacting $InI_3$ with $NaNH_2$, single crystal and highly crystalline InN nanoparticles have been successfully obtained in benzene–thermal systems. This reaction route provides an alternative method for successful synthesis of high-quality InN without the coexistence of other impurities, such as In, $In_2O_3$ *etc.* Notably, by controlling the parameters of reaction temperature and time, nanoparticles of different sizes were obtained in the final products.

## Experimental

### The preparation of indium iodide

Indium iodide ($InI_3$) was prepared by the reaction of 6 mmol metallic In and 12 mmol iodine ($I_2$) in a 1 : 2 molar ratio in a 50 mL Telfon-lined autoclave, which is filled with anhydrous benzene (pretreated by Na metal for 30 min to remove $H_2O$) up to 95% of its total volume. The autoclave was sealed and maintained at 210 °C for 5 h, then allowed to cool to room temperature naturally. An instant precipitation was observed. The yellow precipitate was washed with anhydrous benzene and then dried under vacuum at 30 °C for 4 h. The reaction process can be represented by:

$$2In + 3I_2 \rightarrow 2InI_3 \quad (1)$$

Since $InI_3$ can be dissolved in benzene, it is reasonable to believe that the as-obtained $InI_3$ is produced by a recrystallization process. Apparently, when the amount of In metal is lower than 3 mmol, there are no solid precipitates obtained. Additionally, the appropriate ratio of $[I_2]/[In]$ is also essential to the quality of $InI_3$. When the ratio of $[I_2]/[In]$ is larger than 3 : 1, a black slurry is obtained, rather than the yellow solid obtained at a ratio of 2 : 1. Reacting In with insufficient $I_2$ (<1 : 1) leads to the coexistence of metallic In and $InI_3$.

### The preparation of indium nitrides

The as-obtained $InI_3$ (3 mmol) and 9 mmol $NaNH_2$ were added into a 50 ml Telfon-lined autoclave filled with anhydrous benzene up to 95% of its total volume. The autoclave was sealed and maintained at a certain temperature (180 °C, 210 °C, 230 °C) for the desired reaction time. The black precipitate was filtered and washed with absolute ethanol and distilled water in sequence, and then dried under vacuum at 50 °C for 2 h.

$$InI_3 + 3NaNH_2 \rightarrow InN + 3NaI + 2NH_3 \quad (2)$$

### Structure characterization, composition analysis, and optical properties

X-Ray powder diffraction (XRD) was performed with a Philips X'Pert Pro Super diffractometer with Cu Kα radiation ($\lambda$ = 1.54178 Å). The transmission electron microscopy (TEM) images were performed with a Hitachi Model H-800 instrument with a tungsten filament, using an accelerating voltage of 200 kV. The selected-area electron diffraction (SAED) patterns and high-resolution transmission electron microscopy (HRTEM) images were carried out on a JEOL –2010 TEM at an acceleration voltage of 200 KV. X-Ray photoelectron spectroscopy (XPS) measurements were performed on a VGESCALAB MKII X-ray photoelectron spectrometer with an exciting source of Mg Kα = 1253.6 eV. Raman spectra and photoluminescence spectroscopy (PL) were recorded at room temperature with a LABRAM-HR Confocal Laser Micro-Raman Spectrometer using 514.5 nm excitation wavelength. Absorption spectra were recorded using a Shimadzu UV-365 UV-VIS-NIR Recording Spectrophotometer. The samples were dried at 80 °C under vacuum for 6 h and then dispersed in anhydrous toluene and recorded in the 400–1600 nm region.

## Results and discussion

X-Ray powder diffraction (XRD) patterns reveal the phase and purity of the as-obtained products. Here, the as-obtained products for the direct reaction of $InI_3$ and $NaNH_2$ at different temperature of 210 °C and 230 °C and different reaction times of 5 h and 24 h were investigated, and the obtained samples were correspondingly named InN210-5, InN210-24, InN230-5, and InN230-24, respectively. It can be seen that the full-range XRD patterns of the products for the high-quality InN nanocrystals are all identical. As is shown, there are sets of Bragg peaks in the full-range XRD that could readily be indexed to be a pure hexagonal phase InN (3.544 ± 0.003 Å, $c$ = 5.705 ± 0.007 Å) and which was well crystalline for these four patterns, respectively. No impurity peaks from elemental In, $In_2O_3$, or $InI_3$ were found in the experimental range. Furthermore, the magnified (101) peak is displayed in Fig. 1B, from which one can see that the peak (101) becomes narrower in the sequence of Fig. 1A (a–d), clearly indicating that size evolution occurs. Employing the Scherrer equation from the full width at half-maximum (FWHM) of the (100), (101) and (110) reflections, the mean crystalline sizes for Fig. 1A (a–d) are 9.8 nm, 14.8 nm, 20.6 nm, and 36.0 nm respectively, which are consistent with the particle size of InN nanoparticles or the diameters of nanorods in the following TEM observation.

Further evidence for purity and composition of the sample is obtained by XPS measurements. The typical survey spectrum (Fig. 2A) indicates the presence of In and N, as well as C from the reference and O impurity from absorbed gaseous molecules, and the absence of any impurity such as I or Na. Higher resolution spectra were also recorded in the In 3d (Fig. 2B) and N 1s (Fig. 2C) regions. The In core spin–orbit split to the $3d_{5/2}$ peak at 443.6 eV and $3d_{3/2}$ peak at 451.2 eV can be seen. The peak at around 396.3 eV corresponds to N 1s of InN. These

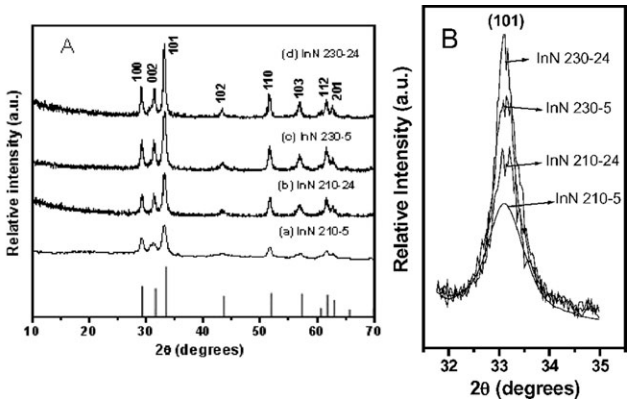


**Fig. 1** (A) Powder XRD patterns of the as-obtained InN nanocrystals obtained at 210 °C for 5 h (a) and 24 h (b); 230 °C for 5 h (c), 24 h (d) and the standard JCPDS card for pure InN as a reference (No. 74–0244). (B) The magnified (101) peaks for these four samples.

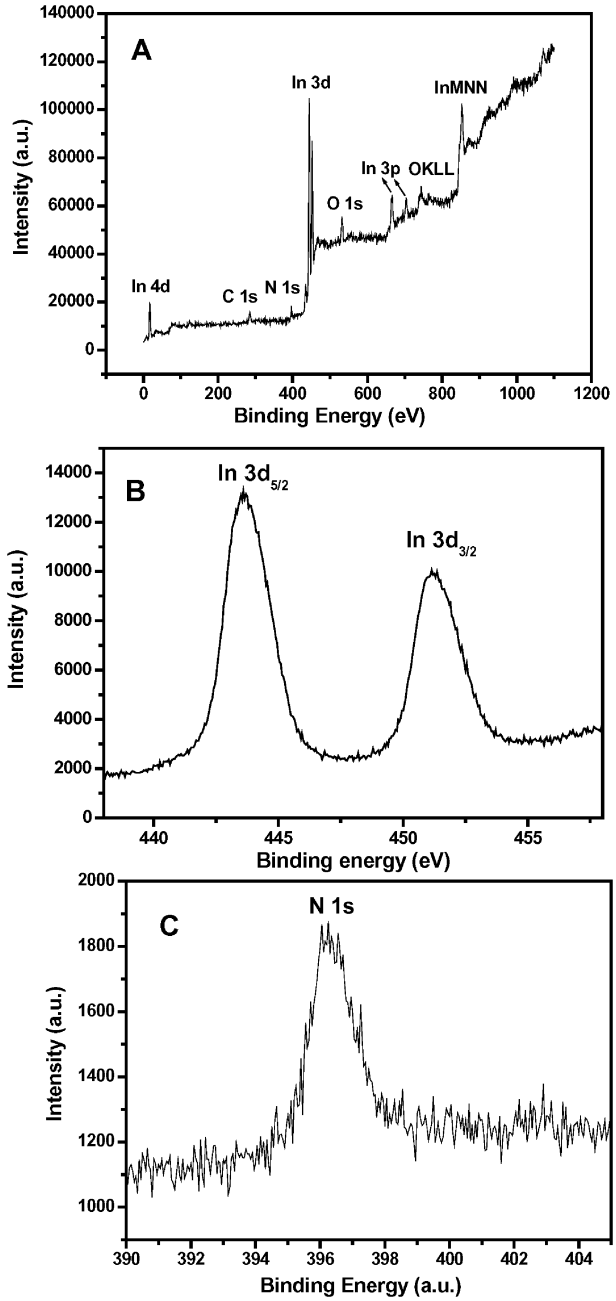


**Fig. 2** Typical XPS spectra of the sample obtained by the direct reaction of $InI_3$ and $NaNH_2$ at 210 °C for 24 h. (A) Survey region, (B) higher resolution In 3d region and (C) higher resolution N 1s region.

results are in good agreement with the values of bulk InN in the literature.[14] The average atomic ratio of In to N is around 1.042 : 1 on the basis of the quantification of the $In_{3d}$ and $N_{1s}$ peaks. Another three hexagonal InN (h-InN) samples with atomic ratios of 1.050 : 1, 1.142 : 1, and 1.120 : 1 were also prepared at 210 °C for 5 h (InN210-5), 230 °C for 5 h (InN230-5), and 230 °C for 24 h (InN230-24), respectively. These experimental data were close to the stoichiometry of InN.

The TEM image of the sample obtained at 210 °C for 5 h revealed the formation of relative uniform nanoparticles with sizes about 9.6 nm ± 4 nm (Fig. 3a). Fig. 3b gives a profile HRTEM image of an InN nanocrystal, which shows it to be a single crystal and well crystalline. The lattice distance is 3.06 Å, indicating the (100) plane. Most nanoparticles (>96%) are single crystalline. Reacting at 210 °C for 24 h and 230 °C for 5 h produced nanoparticles of 14.5 nm ± 4 nm and 22.0 nm ± 6 nm, respectively (Fig. 3c and Fig. 4a). Fig. 4b–d are the HRTEM images of three particles with clear interplanar

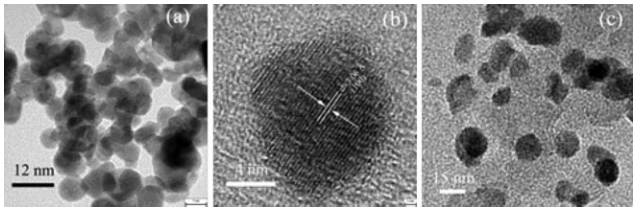


**Fig. 3** (a–b) TEM image and HRTEM images of the nanoparticles obtained at 210 °C for 5 h. (c) TEM image of the nanoparticles obtained at 230 °C for 24 h.

distances of 2.85 Å and 2.69 Å, matching well with the $d_{002}$ and $d_{101}$ spacing of wurtzite-type InN, respectively. The 61.8° orientation between the (002) and (101) lattice planes is consistent with the crystal structure (Fig. 4b). Selected area electron diffraction patterns (inset in Fig. 4b) can be indexed to hexagonal crystal structure of InN, confirming the hexagonal crystal structure of InN. However, on careful observation of the boundary of these three particles, it is found that they share common crystallographic planes between two particles (Fig. 4c), sharing the (101) and (002) planes between the particles, indicating that orientation–attachment occurs in this case. In the orientation–attachment process, adjacent nanoparticles are self-assembled by sharing a common crystallographic orientation and docking of these particles at a planar interface.[15] In the past decade, an increasing number of examples, which are relevant to such a mechanism, have been reported such as $\alpha$-$Fe_2O_3$,[16] Au,[17] hydroxyapatite ($Ca_{10}(PO_4)_6(OH)_2$),[18] $TiO_2$,[19] FeOOH,[20] CoOOH,[21] ZnS[22] and $ZnWO_4$.[23] However, as far as we know, there are no metal nitrides found possessing such a mechanism, and thus, this is the first example of orientation–attachment occurring between particles for the nitrides. Obviously, this observation also provides the possibility of synthesis of one-dimensional InN *via* an orientation–attachment process, like that for ZnO[24] *etc.* Evidently, at 230 °C and the longer reaction time of 24 h, besides the larger particles in the final products (Fig. 5a), some nanorods were also found (Fig. 5b–c). Although the yield of nanorods is relatively low (15%), this demonstrated the possibility of the synthesis of InN one-dimensional nanostructures *via* an orientation–attachment process, which is different from the conventional routes for one-dimensional nitrides in previous reports.[5] In a word, it can be found that longer reaction time and higher reaction temperature lead to an increase in the particle size based on the TEM analysis: as for the reaction temperature: 210 °C: 14.5 nm

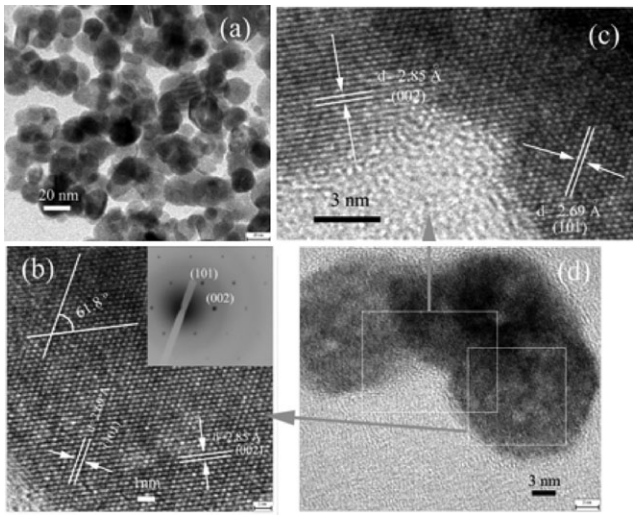


**Fig. 4** TEM image (a) and HRTEM images (b–d) of the nanoparticles obtained at 230 °C for 5 h. HRTEM images revealed that orientation–attachment occurs between the InN particle and particle (b–d).

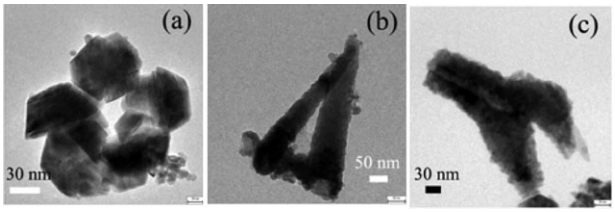


**Fig. 5** TEM image of a mixture of nanoparticles (a) and nanorods (b–c) obtained at 230 °C for 24 h.

(24 h) > 9.6 nm (5 h); 230 °C: 35.1 nm (24 h) > 22.0 nm (5 h); as for the reaction time of 5 h, 22.0 nm (230 °C) > 9.6 nm (210 °C); 24 h: 35.1 nm (230 °C) > 14.5 nm (210 °C), which were consistent with the XRD results from the Scherrer equation.

Our approach to h-InN is essentially based on the reaction between $InI_3$ and $NaNH_2$, and according to the enthalpy calculations, eqn. (2) is thermodynamically spontaneous and highly exothermic ($\Delta H_r^\circ = -539.05$ kJ mol$^{-1}$).[25] However, in most other cases, the reactions are almost instantaneous and the products obtained were a fused mass rather than an ultrafine powder due to the inability to release as-produced energy from the system.[26] In our present route, the benzene solvent can absorb the reaction enthalpy released from this process and maintain a relatively low overall reaction temperature.[27] So, the products prepared were nanosized rather than fused. Furthermore, under our reaction conditions, $InI_3$ can be dissolved in benzene to form a solution and notably, the melting point of $NaNH_2$ is 210 °C, indicating that the In source and nitrogen source should be well dispersed in benzene–thermal systems, resulting in free-standing nanoparticles in the final products.

To investigate the effect of reaction conditions on the formation of InN single crystals, a series of relevant experiments were carried out through similar processes and summarized in Table 1 It is obvious that the reaction temperature, relevant indium source and nitrogen source played a critical role in the formation of InN single crystals. Lower temperatures than 200 °C could not initiate reaction and higher temperatures resulted in larger particles and rods. When $InBr_3$ was substituted for $InI_3$ as the In source keeping the other reaction parameters constant, only metallic In was obtained. This result may be related to the stronger covalent ability of $InI_3$ than $InBr_3$, preventing the $InI_3$ from being reduced to metallic In as for $In_2S_3$.[8] Additionally, only metallic In was obtained if $Li_3N$ was substituted for $NaNH_2$ as the nitrogen source, indicating the stronger reducing ability of $Li_3N$ compared with that for $NaNH_2$.

The above characterization of the typical InN samples contained only the hexagonal phase, and their nanoparticles appear excellently single-crystalline. Further, the as-obtained

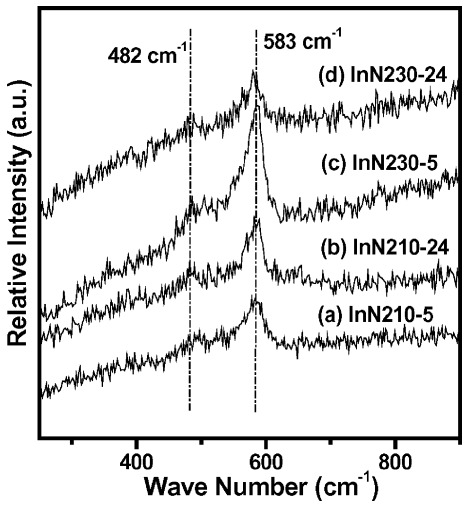


**Fig. 6** Raman spectra of the as-obtained InN nanocrystals obtained at 210 °C for 5 h (a) and 24 h (b); 230 °C for 5 h (c) and 24 h (d).

products possess no iodine or amorphous layers on the surface of the particles as revealed by the XPS and HRTEM results, respectively, indicating the high purity of the InN nanoparticles in our work. Additionally, there is no surfactant involved in our synthetic procedure which avoids the possibility of background spectral features arising from additional surfactants (such as TOPO[7]), facilitating our investigation of the optical properties of the InN nanoparticles. The availability of such samples was important for the observation of allowed optical phonons and their symmetry assignment both in Raman and IR measurements, as well as the optical bandgap energy in the absorbance spectrum. Here the four typical samples were investigated for the following optical properties, *i.e.* InN210-5, InN210-24, InN230-5, and InN230-24, respectively.

The hexagonal wurtzite InN crystal structure belongs to the space group $C_{6v}$,[4] and the group theory analysis predicts the zone-center optical modes $A_1 + 2B_1 + E_1 + 2E_2$. Among them, the $A_1$ and $E_1$ modes are both Raman and infrared active, the two $E_2$ modes are only Raman active, and while the $B_1$ modes are silent, *i.e.*, forbidden in Raman Scattering. Fig. 6 shows the Raman spectra of four typical samples. The Raman spectra are similar in all four samples, and two peaks can be found: a strong peak centered at 583 cm$^{-1}$ and a weak peak centered at 482 cm$^{-1}$ which can be assigned to $E_2^2$ and A1 (LO), respectively.[28] Notably, the reason why the $E_2^2$ peak is weak is that the $E_2$ phonon is commonly not as strongly affected by resonance excitation conditions as a non-polar phonon.[29] We have also measured the IR spectra of these four samples as shown in Fig. 7. From the full-range IR spectra ranging from 400 to 3700 cm$^{-1}$, it is found that there are broad absorptions

**Table 1** A Summary of direct reactions between different In-source and nitrogen-source at a low temperature

| Reactants | Reaction temperature | Reaction time | Product | Morphology and size |
|---|---|---|---|---|
| 6 mmol $InI_3$ 18 mmol $NaNH_2$ | <190 °C | 1 day | Amorphous products | — |
| | 210 °C | 5 h | InN | Particles, 9.6 nm ± 5 nm |
| | 210 °C | 24 h | InN | Particles, 14.5 nm ± 5 nm |
| | 230 °C | 5 h | InN | Particles, 22.0 nm ± 6 nm |
| | 230 °C | 24 h | InN | Particles, nanorods 35.1 nm ± 10 nm |
| 6 mmol $InI_3$ 6 mmol $Li_3N$ | 210 °C | 24 h | In | — |
| | 230 °C | 24 h | In | — |
| 6 mmol $InBr_3$ 18 mmol $NaNH_2$ | 210 °C | 24 h | In | — |
| | 230 °C | 24 h | In | — |

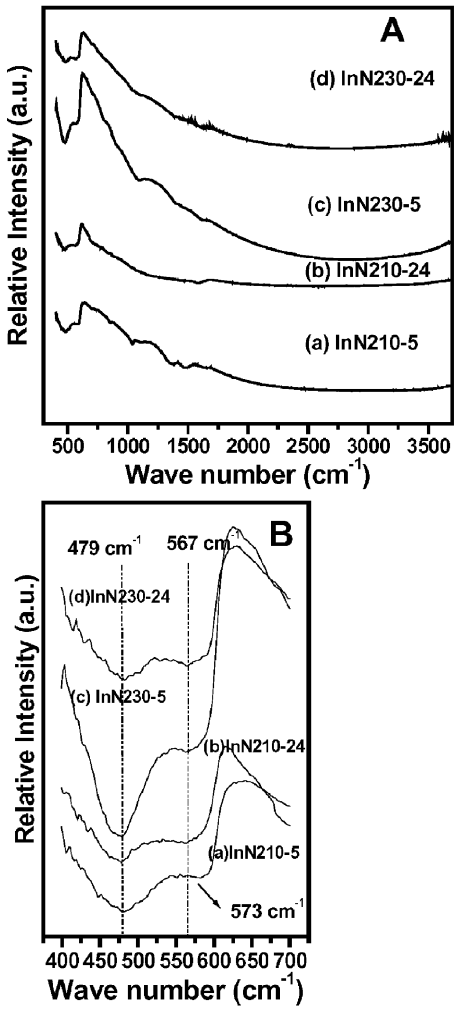


**Fig. 7** Full-range IR spectra and partial-range (400–700 $cm^{-1}$) of the as-obtained InN nanocrystals obtained at 210 °C for 5 h (a) and 24 h (b); 230 °C for 5 h (c) and 24 h (d).

in the range 400–700 $cm^{-1}$ as shown in Fig. 7A, indicating the characteristic absorption of indium nitride.[8] On careful observation in the IR range 400–700 $cm^{-1}$ (Fig. 7B), two absorption peaks for each sample can be found: absorption peaks at 479 $cm^{-1}$ and around 570 $cm^{-1}$ (three at 567 $cm^{-1}$ and one at 573 $cm^{-1}$) can be assigned to $E_1$(TO) and $E_1$(LO), respectively.[30] By combined analysis of Raman and IR results, our experimental data were consistent with the theoretical prediction that the $A_1$ and $E_1$ modes are both Raman and infrared

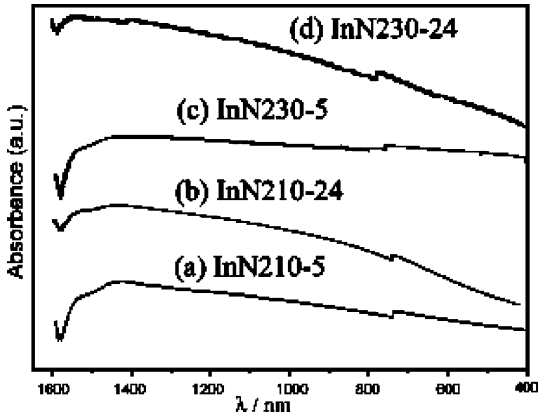


**Fig. 8** Absorption spectra for the as-obtained InN nanocrystals obtained at 210 °C for 5 h (a) and 24 h (b); 230 °C for 5 h (c) and 24 h (d).

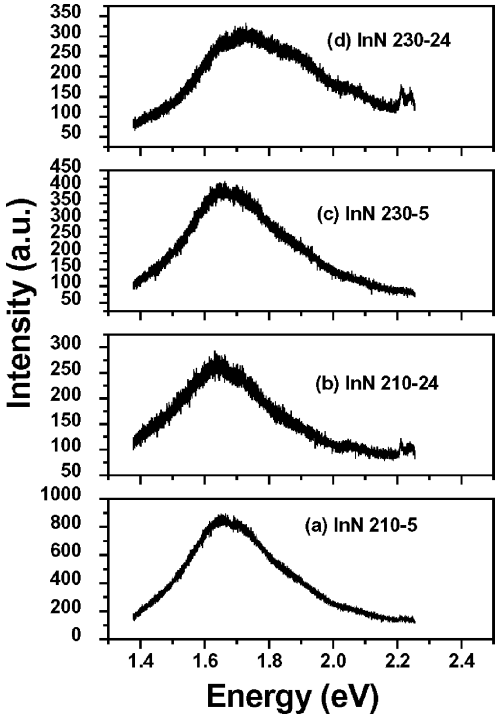


**Fig. 9** Photoluminescence spectra for the as-obtained InN nanocrystals obtained at 210 °C for 5 h (a) and 24 h (b); 230 °C for 5 h (c) and 24 h (d).

active and the two $E_2$ modes are only Raman active. Meanwhile, this gives further evidence that high quality InN nanocrystals were obtained.

Theoretical calculations show that the intrinsic bandgap of InN is ~0.65 eV and the 1.9 eV band has been considered to arise from oxygen incorporation.[31] As is reported, the intrinsic bandgap of InN is in the 0.7–0.8 eV range, rather than the commonly reported 1.9 eV.[32] Furthermore, the different electron concentrations could lead to the variation in bandgap between 0.7 and 1.7 eV.[33] In this case, the as-obtained InN nanocrystals with different sizes all show a characteristic sharp band centered at about 1590 nm (*i.e.* ~0.78 eV) in the near-IR region (0.7–0.8 eV) (Fig. 8). Given the absence of a clear band centered around 1.9 eV in such samples, it is reasonable to believe the intrinsic bandgap is 0.7 eV, rather than 1.9 eV in the current work. Notably, this result gives us a fine example for understanding the exact intrinsic bandgap for InN, since high quality InN was obtained here at a low temperature range (<250 °C). Additionally, the 1.7 eV PL band (Fig. 9) arising from defects is known to be characteristic of InN.[34]

## Conclusion

In conclusion, we present our preliminary findings that single crystal and highly crystalline InN nanoparticles can be synthesized by directly reacting $InI_3$ with $NaNH_2$ in benzene–thermal systems, and this represents the first example of the direct synthesis of high-quality InN using indium halide as the In source. Additionally, it was found that longer reaction time and higher reaction temperature led to an increase in particle size and thus InN nanoparticles with different size distributions can also be obtained. The orientation–attachment process was observed between InN particles. To the best of our knowledge, this is the first example of an orientation–attachment process occurring in nitride primary particles, and one-dimensional InN appeared at longer reaction times *via* the orientation–attachment process. Raman and IR results indicated that our experimental data were consistent with the theoretical prediction, and this gives further evidence that high quality InN nanocrystals were obtained. Moreover, it has been shown that

the near-infrared band around 0.7 eV is characteristic of these materials.

## Acknowledgements

This work was supported by the National Natural Science Foundation of China and the Chinese Ministry of Education.

## References


1 (*a*) T. Matsuoka, *Adv. Mater.*, 1996, **8**, 469–479; (*b*) F. A. Ponce and D. P. Bour, *Nature*, 1997, **386**, 351–359; (*c*) S. Nakamura, *Science*, 1998, **281**, 956–961.
2 T. Matsuoka, H. Okamoto, M. Nakao, H. Harima and E. Kurimoto, *Appl. Phys. Lett.*, 2002, **81**, 1246.
3 S. H. Wei, X. L. Nie, I. G. Batyrev and S. B. Zhang, *Phys. Rev. B*, 2003, **67**, 165209.
4 (*a*) D. A. Neumayer and J. G. Ekerdt, *Chem. Mater.*, 1996, **8**, 9–25; (*b*) I. Akasaki and H. Amano, *J. Cryst. Growth*, 1995, **146**, 455–466.
5 L. W. Yin, Y. Bando, D. Golberg and M. S. Li, *Adv. Mater.*, 2004, **16**, 1833.
6 S. D. Dingman, N. P. Rath, P. D. Markowitz, P. C. Gibbons and W. E. Buhro, *Angew. Chem., Int. Ed.*, 2000, **39**, 1470–1472.
7 P. S. Schofield, W. Z. Zhou, P. Wood, I. D. W. Samuel and D. J. Cole-Hamilton, *J. Mater. Chem.*, 2004, **14**, 3124.
8 J. Xiao, Y. Xie, R. Tang and W. Luo, *Inorg. Chem.*, 2003, **42**, 107–111.
9 Y. Xie, Y. T. Qian, W. Z. Wang, S. Y. Zhang and Y. H. Zhang, *Science*, 1996, **272**, 1926.
10 R. L. Wells and J. F. Janik, *Eur. J. Solid State Inorg. Chem.*, 1996, **33**, 1076.
11 Y. J. Bai, Z. G. Liu, X. G. Xu, D. L. Cui, X. P. Hao, X. Feng and Q. L. Wang, *J. Cryst. Growth*, 2002, **241**, 189.
12 R. W. Cumberland, R. G. Blair, C. H. Wallace, T. K. Reynolds and R. B. Kaner, *J. Phys. Chem. B*, 2001, **105**, 11922.
13 Y. H. Zhang, *Inorg. Chem.*, 1982, **21**, 3886.
14 Y. Lu, L. Ma and C. Lin, *J. Vac. Sci. Technol., A*, 1993, **11**, 2931.
15 R. L. Penn and J. F. Banfield, *Science*, 1998, **281**, 969–971.
16 (*a*) J. K. Bailey, C. J. Brinker and M. L. Mecartney, *J. Colloid Interface Sci.*, 1993, **157**, 1–13; (*b*) M. Ocana, M. P. Morales and C. J. Serna, *J. Colloid Interface Sci.*, 1995, **171**, 85–91.
17 V. Privman, D. V. Goia, J. Park and E. Matijevi, *J. Colloid Interface Sci.*, 1999, **213**, 36–45.
18 K. Onuma and A. Ito, *Chem. Mater.*, 1998, **10**, 3346–3351.
19 A. Chemseddine and T. Moritz, *Eur. J. Inorg. Chem.*, 1999, 235–245.
20 R. L. Penn, G. Oskam, T. J. Strathmann, P. C. Searson, A. T. Stone and D. R. Veblen, *J. Phys. Chem. B*, 2001, **105**, 2177–2182.
21 R. L. Penn, A. T. Stone and D. R. Veblen, *J. Phys. Chem. B*, 2001, **105**, 4690–4697.
22 F. Huang, H. Z. Zhang and J. F. Banfield, *Nano Lett.*, 2003, **3**, 373–378.
23 B. Liu, S. H. Yu, L. J. Li, F. Zhang, Q. Zhang, M. Yoshimura and P. K. Shen, *J. Phys. Chem. B*, 2004, **108**, 2788–2792.
24 C. Pacholski, A. Kornowski and H. Weller, *Angew. Chem., Int. Ed.*, 2002, **41**, 1188–1191.
25 *Lange's Handbook of Chemistry*, 13th edn, ed. J. A. Dean, McGraw-Hill, New York, 1985.
26 A. L. Hector and I. P. Parkin, *Polyhedron*, 1995, **14**, 913.
27 J. Q. Hu, Q. Y. Lu, K. B. Tang, B. Deng, R. R. Jiang, Y. T. Qian, G. E. Zhou and X. M. Liu, *Chem. Lett.*, 2000, **29**, 74–75.
28 (*a*) M. Kuball, J. W. Pomeroy, M. Wintrebert-Fouquet, K. S. A. Butcher, H. Lu and W. J. Schaff, *J. Cryst. Growth*, 2004, **269**, 59; (*b*) A. G. Bhuiyan, A. Hashimoto and A. Yamamoto, *J. Appl. Phys.*, 2003, **94**, 2779.
29 D. Behr, J. Wagner, J. Schneider, H. Amano and I. Akasaki, *Appl. Phys. Lett.*, 1996, **68**, 2404.
30 T. Inushima, T. Shiraishi and V. Y. Davydoc, *Solid State Commun.*, 1999, **110**, 491.
31 A. G. Bhuiyan, A. Hashimoto and A. Yamamoto, *J. Appl. Phys.*, 2003, **94**, 2779.
32 J. Wu, W. Walukiewicz, K. M. Yu, J. W. Ager III, E. E. Haller, H. Lu, W. J. Schaff, Y. Saito and Y. Nanishi, *Appl. Phys. Lett.*, 2002, **80**, 3967.
33 G. Kaczamarczyk, A. Kaschner, S. Reich, A. Hoffmann, C. Thomsen, D. J. As, A. P. Lima, D. Schikora, K. Lischka, R. Averbeck and H. Riechert, *Appl. Phys. Lett.*, 2000, **76**, 2122.
34 C. H. Liang, L. C. Chen, J. S. Hwang, K. H. Chen, Y. T. Hung and Y. F. Chen, *Appl. Phys. Lett.*, 2002, **81**, 22–24.